Double Peak-Induced Distance Error in STFT-BOTDR Event Detection and the Recovery Method

YIFEI YU, LINQING LUO, BO LI, LINFENG GUO, JIZE YAN* AND KENICHI SOGA

Department of Engineering, University of Cambridge, Trumpington Street, Cambridge, CB2 1PZ, UK
**Corresponding author: yanjize@gmail.com*

Received XX Month XXXX; revised XX Month, XXXX; accepted XX Month XXXX; posted XX Month XXXX (Doc. ID XXXXX); published XX Month XXXX

The measured distance error caused by double peaks in the BOTDRs (Brillouin optical time domain reflectometers) system is a kind of Brillouin scattering spectrum (BSS) deformation, discussed and simulated for the first time in the paper. Double peak, as a kind of Brillouin spectrum deformation, is important in the enhancement of spatial resolution, measurement accuracy and crack detection. Due to the variances of the peak powers of the BSS along the fibre, the measured starting point of a step-shape frequency transition region is shifted and results in distance errors. Zero-padded Short-Time-Fourier-Transform (STFT) can restore the transition-induced double peaks in the asymmetric and deformed BSS, thus offering more accurate and quicker measurements than the conventional Lorentz-fitting method. The recovering method based on the double-peak detection and corresponding BSS deformation can be applied to calculate the real starting point, which can improve the distance accuracy of the STFT-based BOTDR system.

1. Introduction

The Brillouin scattering-based optical fibre sensors can provide a convenient method of health monitoring for large civil structures, such as pipe lines, bridges, tunnels and dams, which is significant for diagnosing deterioration and preventing disasters. BOTDRs (Brillouin optical time domain reflectometers) have been applied to measure the distributed temperature and strain along the entire optical fibre up to 30km, by utilizing the proportionality between the strain and temperature in an optical fibre and the Brillouin frequency shift [1-4]. In the BOTDR system, a laser probing pulse is launched into the sensing fibre and its spontaneous Brillouin scattering (SpBS) spectrum along the fibre is detected at the same end of the fibre, which is convenient for the field applications [4, 5]. Conventionally, the BOTDR system requires a time-consuming frequency scanning of the entire SpBS spectrum and a great amount of averaging up to 2^20 times to obtain the accurate Brillouin scattering spectrum (BSS) by Lorentz fitting [6, 7].

Recently, a fast-speed Discrete Fourier Transform (DFT)-based BOTDR has used the wideband detection architecture accelerated by digital signal processing (DSP) and/or field-programmable gate array (FPGA) to replace the time-consuming frequency sweeping method and takes only 1 s to measure the frequency-down-converted SpBS signal up to 500 MHz over the 1.5 km testing fibre [6, 8]. This wideband detection has been demonstrated at a temperature resolution of 3 °C and a spatial resolution of 2 m for 6 km fibre [10]. Very recently, the distributed dynamic strain measurement has been demonstrated, which can detect 16.7 Hz dynamic strain variation with 4 m spatial resolution and 45 με uncertainty on a 12 m section at the end of a 270 m sensing fibre [11]. In both the traditional BOTDR and DFT-based BOTDR, the centre frequency of the BSS is measured by the peak power of the SpBS spectrum, which assumes that the spectrum is Lorentz shape. If the strain and/or temperature along the fibre under test does not distribute uniformly within the spatial resolution, the actually measured Brillouin spectrum will deform from the Lorentz distribution [12]. Moreover, double BSS peaks exist in the frequency transition region [13-16], which can induce BSS deformation. The detection error of the peak power can therefore deteriorate the distance measurement accuracy of the BOTDR. Hence, the double-peak spectrum deformation is important in improving measurement accuracy [14], spatial resolution [17] and crack detection [18]. However, this effect has not been thoroughly investigated yet.

This paper demonstrated the use of the zero-padding-enhanced Short-Time-Fourier-Transform (STFT) for the first time to restore the spectrum deformation in order to reduce the distance error for a step-shape and uniformly distributed temperature event. A method using three zero crossings of the derivative of BSS along the distance axis over the transition area is utilised to verify the existence of double peaks. The measured starting point of the events is shifted within the effective pulse length due to the power variance in the two events. A recovery method is introduced to compensate the distance error by applying the measured power variances of the BSS into its integration solutions.

In this paper, section 2 reviews the BSS; section 3 describes the origin of the double peaks as a kind of spectrum deformation, the

induced distance error and the method to determine double peaks. In section 4, the advantages of zero-padded STFT is explained with the potential to replace the conventional frequency-sweeping and Lorentz-fitting method. The recovery method is introduced in Section 5. Section 6 describes the experimental results and discussions.

2. BSS in the fibre

Brillouin scattering results from the scattering of light by sound waves [19]. The exponential decay of the acoustic waves results in a gain representing a Lorentz-shape profile [20]:

$$g(\nu,\nu_B) = g_0 \frac{\Delta\nu^2}{(\nu-\nu_B)^2 + \Delta\nu^2} \quad (1)$$

Where g_0 is a Brillouin gain coefficient, $\Delta\nu$ is the half-width at half-maximum and ν_B is the central frequency at peak-power. It was found that the SpBS frequency increases linearly with strain [21] and temperature [22]:

$$\nu_B(\varepsilon) = \nu_B(0)[1+C_s\varepsilon] \quad (2)$$

$$\nu_B(t) = \nu_B(t_r)[1+C_t(t-t_r)] \quad (3)$$

Where ε is the tensile strain, t is the temperature and t_r is reference temperature, respectively.

3. Double-peaks-induced distance error in BOTDR

The spatial resolution of a BOTDR system is affected by both the light pulse duration and detection bandwidth. The spatial resolution δz is given by [23]:

$$\delta z = \max\left\{\frac{cW}{2n}, \frac{cN}{2nf_s}\right\} \quad (4)$$

Where W is the pulse width, c is the speed of light in vacuum, n is the refractive index of the fibre core, N is the number of DFT points in a frame and fs is the sampling rate. A short pulse increases the spatial resolution, but the BSS broadens at the same time [16]. If the number of DFT points decrease in a frame, the waveform frequency resolution will worsen.

As the light pulse travels along the fibre, the BSS will be built by the sum of the components generated in a fibre within the effective pulse length [14]. Fig. 1 summarises the evolution of double peaks in BSS due to the interaction of light pulse with temperature event transition area in the fibre. As shown in the figure, the BSS only has one peak when the pulse travels in the uniform temperature event.

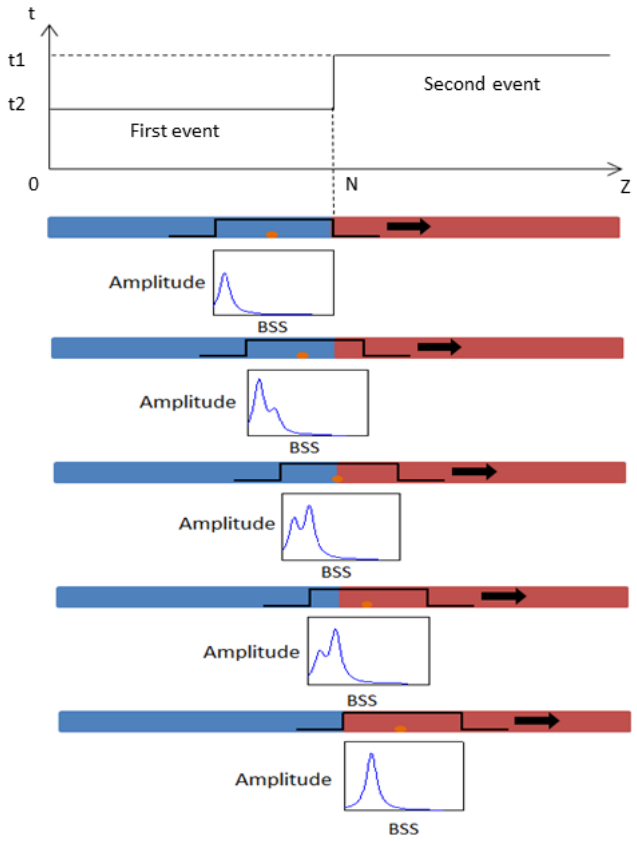

Fig. 1. Schematic of the temperature distribution, the optical pulse and its BSS along the fibre.

When the pulse enters the transition area of the event, the double peaks happen when the peaks are well separated in the spectrum as shown in Fig. 2a. Otherwise, two close peaks can induce Brillouin spectrum deformation as shown in Fig. 2b, and increase the full width at half-maximum (FWHM) of the BSS. Fig. 2 is derived from two Lorentzian-shaped Brillouin gain spectrums and their sum. The phenomenon of double peaks is a source of the BSS deformation, which is displayed in the spectrum domain obtained by digitizing the Brillouin scattering time domain signal and transferring the signals to frequency domain using time-frequency analysis.

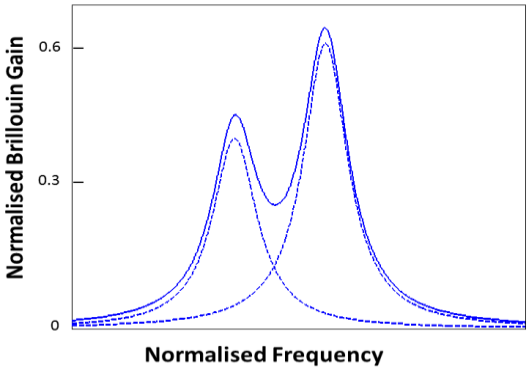

(a)

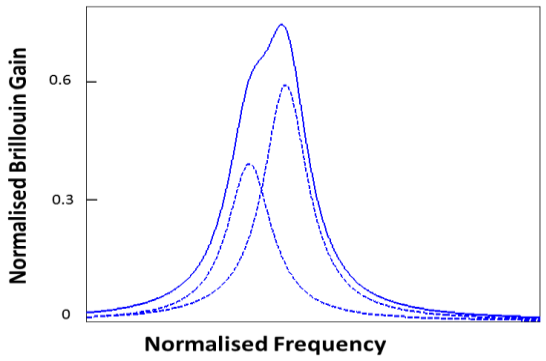

(b)

Fig. 2. (a) Spectrum of double peaks. (b) Spectrum of two close peaks which cannot be well separated.

It is defined that the starting point of the second event happens when the middle of the effective pulse meets the 2nd event [13, 14]. In both events, the temperature is uniformly distributed, with different temperatures t_1 and t_2, respectively. The distribution is given as:

$$t(z) = \begin{cases} t_1 & 0 \le z < N \\ t_2 & N \le z \end{cases} \quad (5)$$

As a result, the light pulse will travel through the step-shape events gradually, which leads to a merging of the two BSSs with different peak-power frequencies within the spatial resolution. Generally, the middle point of the pulse represents the real position of a local strain and/or temperature change [12, 13].

The Brillouin spectrum $H_i(v)$ over the effective pulse can be expressed as the integration of BSS over the effective pulse length:

$$H_i(v) = \int_{z_i - \Delta z/2}^{z_i + \Delta z/2} g(v, v_B(t(z)))dz \quad (6)$$

Where z_i is the centre of the effective pulse, Δz is the length of the effective pulse, $t(z)$ is the temperature at position z. By substituting Eqs (1),(3) and (5) into Eq. (6) the BSS can be rewritten as:

$$G(z) = \int_{z_i - \Delta z/2}^{z_i + \Delta z/2} g(z) \frac{\Delta v^2}{(v - v_B(t(z))(1 + C_t(t - t(z))))^2 + \Delta v^2} dz \quad (7)$$

where $g(z)$ is given by

$$g(z) = \begin{cases} g_1 & 0 \le z < N \\ g_2 & N \le z \end{cases} \quad (8)$$

By solving Eqs. (7) and (8), the BSS as a function of the distance can be derived. Fig. 3 shows a simulated situation of a double-peak 3D BSS within the effective pulse length.

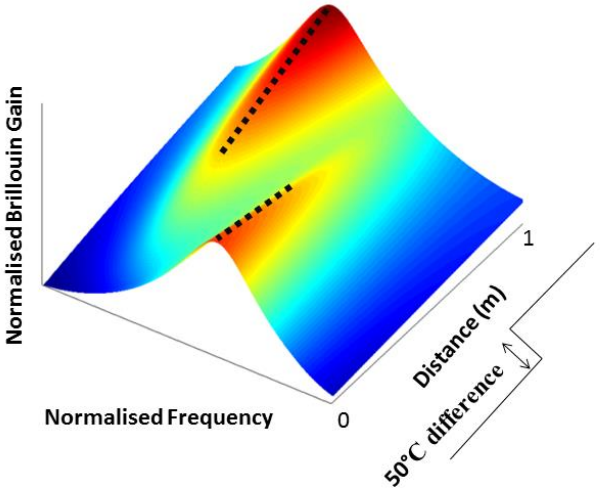

Fig. 3. 3D spectrum of double-peak transition region within effective pulse width.

The double-peaks-induced spectrum deformation will result in a distance error of the measurement. Since the Brillouin centre frequency is obtained by the peak-power detection of the spectrum, in the case that the BSS contains double peaks, the BOTDR system captures the higher peak, which sharpens the detected curve of the peak-power frequency. However, the two peaks of the BSS usually have different Brillouin scattering gains with different temperatures and/or strains [20]; therefore, the detected event transition point (where the peak-power of the two peaks are equal) will not be the real event transition position. The BSS with the higher gain will dominate the spectrum more in the double-peak region, which results in the length extension of the detected event and a distance error of the measurement. As simulated in Fig. 3, a BSS with a higher gain has a larger influence on the spectrum deformation, which induces a distance error using conventional peak-power frequency detection.

The existence of double peaks in the transition region can be actually predicted by solving the differential of the BSS along the distance axis. If there are three zero roots along the distance domain, double peaks exist as simulated in Fig. 3 and Fig. 4.

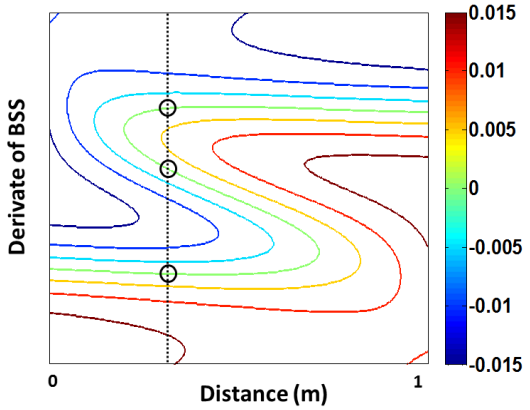

Fig 4. Derivative of the BSS over the transition region along the distance axis to verify the existence of double peaks.

Fig . 5 defines the distance error between the measurement and the real situation. The normalised position error of the event is defined as negative if the event transition point is left shifted, and positive if the point is right shifted. For example, if the second event has a higher temperature than the first event, the peak power of the BSS will be detected earlier (left shifted, or having negative position error). As a result, the measured event transition position is left-shifted or having negative position error.

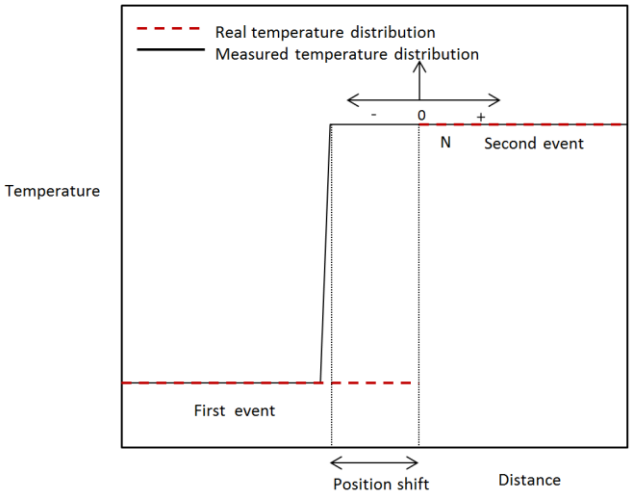

Fig. 5. The red dotted line is the real starting and ending points; the blue line is the simulated Brillouin centre frequency due to pulse and double peaks and the starting and ending.

4. Zero padding-enhanced STFT algorithm

STFT is a transform applied to evaluate the sinusoidal frequency and phase content of local sections of a signal as it changes over time [24]. The signal captured by the digitiser of a coherent heterodyne BOTDR system can be represented as discrete frequency domain information [9]. In the case of a wideband receiver, the data to be transformed need to be split up into frames and each frame is Fourier transformed. The discrete STFT transform is given by [24]:

$$STFT\{x[n]\}(m,\omega) \equiv \sum_{-\infty}^{\infty} x[n]w[n-m]e^{-j\omega n} \quad (9)$$

Where x[n] is the signal to be transformed and w[n] is the window function. DFT requires the signal length to be finite in each frame, which means the N-point DFT operates on an N-elements data vector x[n] to produce an N-element result in a frequency domain X[K].

$$X[k] = \sum_{n=0}^{N-1} x[n] e^{-j2\pi nk/N} \quad (10)$$

If the actual signal length L is less than N, the data vector can be extended by "zero-padding" which accounts to putting zeros at the end of digitised time domain signal [24]. The zero padding will add zeros at the end of original signal x[n] as the following equation:

$$[n] = \begin{cases} v[n], & n = 0,1,2,\ldots L-1 \\ 0, & n = L, L+1,\ldots N-1 \end{cases} \quad (11)$$

The reason to use zero padding is to interpolate the frequency domain signal [25]. As an important step for the recovery methods, zero padding has two advantages. Firstly, it improves the accuracy of transformed spectrum and defines the event detection region more accurately [24]. The conventional fitting method is symmetric, which brings errors in the strain/temperature transition sections [17]. Secondly, the problem of finding the peak of BSS is made easier when the Brillouin spectrum is more densely sampled [26]. It is important to distinguish between two aspects: "spectrum resolution" and "FFT resolution". The spectrum resolution is the minimum spacing between two frequencies that can be resolved. The FFT resolution is the number of points in the spectrum, which is directly proportional to the number of points applied in the FFT.

$$\Delta R_s = \frac{Fs}{L} \quad (12)$$

$$\Delta R_{FFT} = \frac{Fs}{N_{FFT}} \quad (13)$$

N_{FFT} equals the number of actual data and zero padding. Zero padding increases the number of FFT bins per Hz and enhances the accuracy of the peak detection [27]. A robust method for estimating peak frequency is by taking the interpolated peak location in the cross-correlation function as the frequency estimation, which provides much greater immunity to noise [16, 25]. As a summary, due to the asymmetry and deformation of the BSS in the frequency transition region, conventional symmetric Lorentz fitting is not suitable for restoring double peaks in BSS [12, 13]. Zero padding in the time domain corresponds to interpolation in the frequency domain, and interpolating the spectrum is useful in peak detection and asymmetric spectrum restoring [15, 16]. Therefore, zero-padded STFT can restore the spectrum of double peaks and detect the peak-power Brillouin frequency, which is useful for distance error recovering.

5. Distance error recovery method

The recovering method is based on the calculation from Eq. (7) by substituting the BSS gain of the two events and assuming uniformly distributed step-shape temperature events which occupy half and half of the pulse length in the simulation as shown in Fig 6. The calculated BSS, placed in the middle of the effective pulse, is determined by measured Lorentz-shape BSS integration over the effective pulse. The calculated distance error is defined as the difference between the starting points of measured event and the peak power detected from the calculated BBS as shown in Fig. 6. For example, if the measured temperature difference is 50 °C for the step-shape event, and the gain is g_1 and g_2, a step-shape temperature distribution can be placed as shown in Fig. 6A. Integration of the Lorentz-shaped BSS over the length of an effective pulse can bring the calculated BSS over distance as explained in Eq. (7) shown as Fig. 6B. The Brillouin centre frequency shown as the horizontal dash line can be found for both of the measured and calculated BSS along to distance axis, and then the calculated distance error can be worked out.

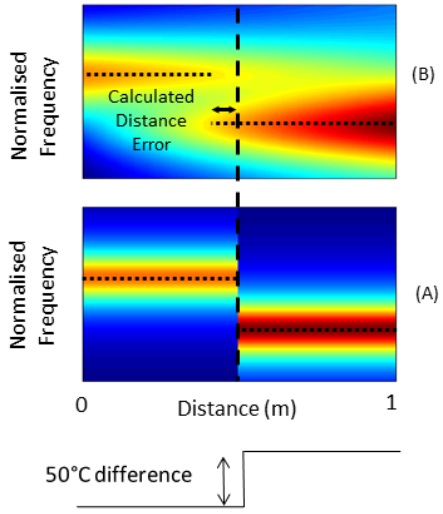

Fig. 6. Calculated distance error, (A) A predefined step-shape temperature event; (B) The estimated BSS calculated by integration over the effective pulse length.

6. Experimental results and discussion

Fig. 7 and 8 show the schematic representation of the STFT based BOTDR system with temperature calibration unit. A continuous-wave (CW) laser diode was followed by a 90/10 coupler which split the light into branch A and B. The branch A signal was modulated by an electro-optical modulator (EOM) with 34 ns modulating pulse. The pulse was amplified by an erbium-doped fibre amplifier (EDFA) followed by an optical filter and then a circulator and launched into a 1.5 km fibre under test (FUT). The branch B was the reference light followed by a polarization scrambler (PS) and then coupled with the back-scattering signal from the FUT. A 26GHz photodetector (PD) is utilized for coherent detection of the system. The PD output was then amplified and frequency down-converted from 10.8 GHz to 350 MHz. A digitizer was utilized to capture the final signal.

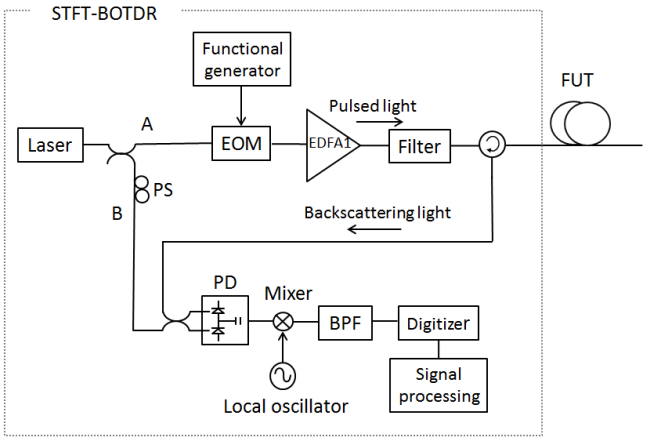

Fig. 7. Experimental setup for STFT-based BOTDR system.
PS: polarization scrambler; EDFA: erbium-doped fibre amplifier; EOM: electro-optic modulator; FUT: fibre under test; BPF: bandpass filter; PD: photodetector.

The total FUT consists of three sections of single mode fibres (SMF) as shown in Fig. 8. The second section is controlled by a waterbath during the experiment. The temperature can be set from 40 °C to 80 °C.

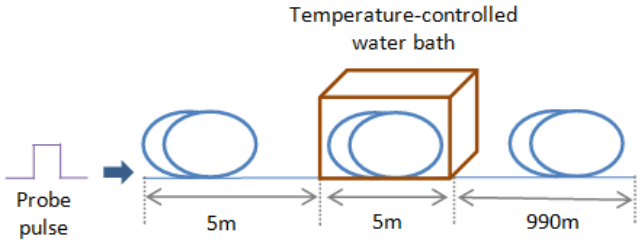

Fig. 8. Experimental setup for the temperature-controlled unit of the STFT-based BOTDR system.

Double peaks have been observed when the temperature in the water bath is higher than 40°C, where the room temperature is 20°C. The BSS measurements in the event transition region at 70°C and 40°C are displayed in Fig. 9 and Fig. 10, respectively. The corresponding derivatives of BSS over the region are shown in Fig. 9b and Fig. 10b, respectively. The window size used in the signal processing was set to be the same as the effective pulse length which is 3.4m, and the spectrum separation is Fs/L = 29.412MHz. In 40°C experiments, the shift of BSS was less than the spectrum separation, so that double-peak was not observed in Fig. 10.

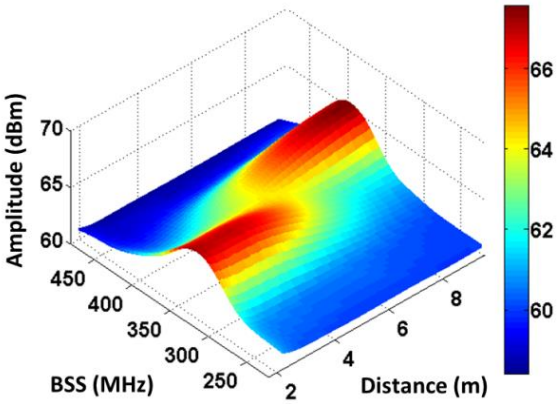

(a)

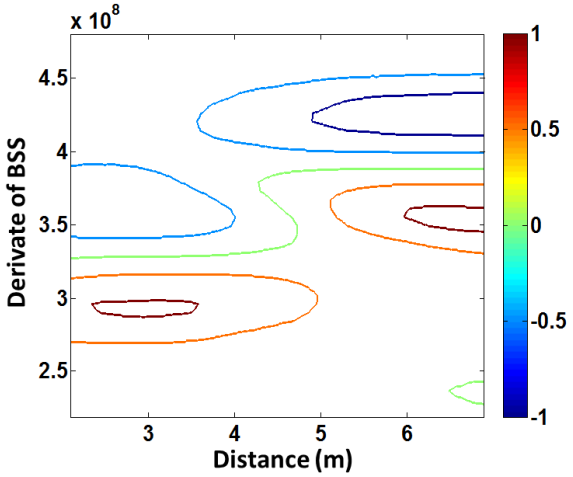

(b)

Fig. 9. Experimental results for 70 °C experiment (a) The plot of BSS along the distance; (b) the derivative of BSS to determine the double peaks.

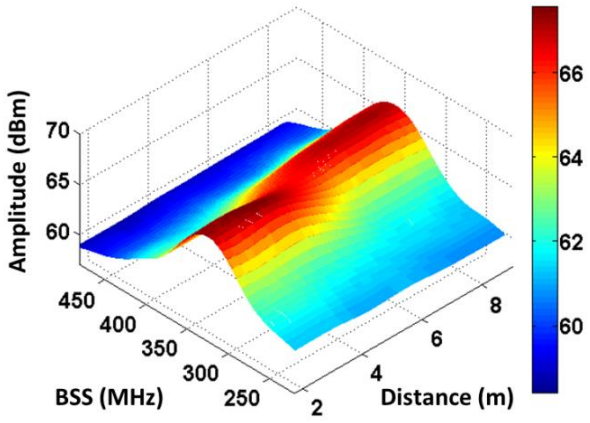

(a)

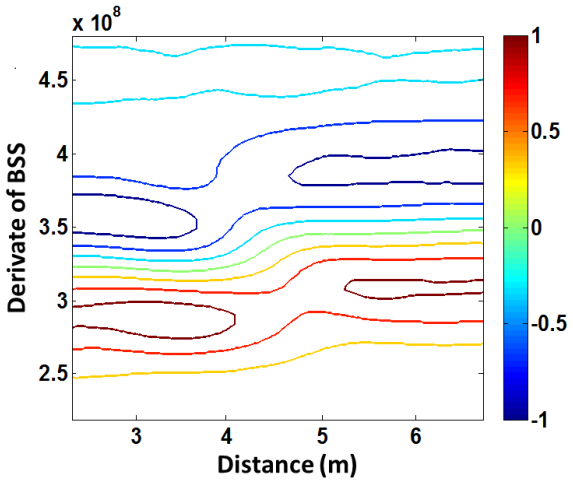

(b)

Fig. 10. Experimental results for 40 °C experiment (a) The plot of BSS along the distance; (b) the derivative of BSS to determine the double peaks.

As the temperature increases, the measured spatial resolution enhances to 0.02 m. The starting point of the section in the waterbath was left-shifted due to the double peaks and has

higher gain at the peak-power frequency than the section in the room temperature. The distance error varies from 0.06m to 0.23m to the left when the temperature rising from 50°C to 80°C and induced left-shift (negative) distance error as shown in Fig. 11. Since the Brillouin gain of the BSS grows as the temperature increases [19], the BSS with higher temperature dominates more and induces larger distance errors.

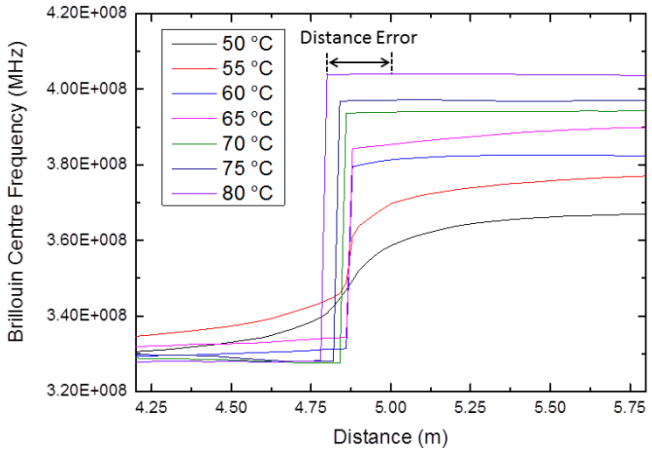

Fig. 11. Experimental results of Brillouin centre frequency from 50 °C to 80 °C.

The measured and calculated distance error is normalised to the effective pulse length (3.4m) shown in Fig. 12 using the recovery method explained in section 5. The difference between the errors is less than 0.3% of the effective pulse length, which indicates that the method can enhance the event position measurement for the step-shape frequency events in the post-processing.

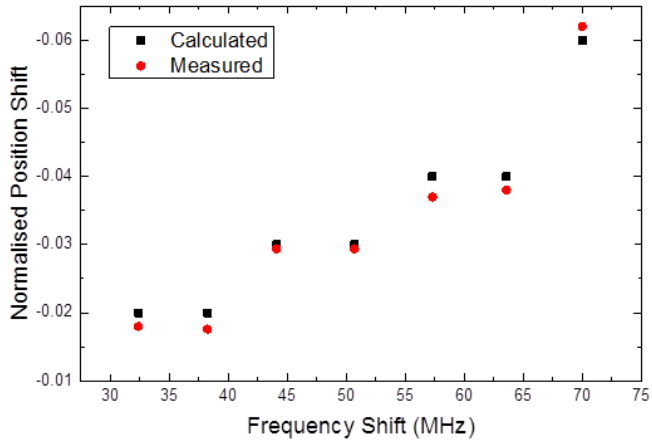

Fig. 12. Normalized position shift with respect to the frequency shift as temperature changes from 50 °C to 80 °C. Square and round points are calculated and measured distance error, respectively.

7. Conclusion

We discussed the distance error of a step-shape temperature distribution in the fibre, which is caused by double-peaks-induced BSS deformation. A zero-padded STFT-BOTDR is demonstrated in the paper as reducing the distance error, which can restore the asymmetric and deforming BSS and offer a more accurate measurement than the frequency sweeping and Lorentz-fitting method used in conventional BOTDR. A method using three zero crossings of the derivative of BSS along the distance axis over the transition area is utilised to verify the existence of double peaks. The measured transition position of the events is shifted due to the BSS power variance in the two events, which can be recovered by applying the measured peak powers of the BSS into a calculation to compensate the position error. Various-shape temperature and strain distribution, such as linear and parabolic shape, can be further investigated as future work.

EPSRC EP/K000314/1 grant is acknowledged. Open data statement: Following on EPSRC policy on research data, the additional data will be accessible at www.repository.cam.ac.uk/handle/1810/247689

References

1. X. Bao and L. Chen, "Recent Progress in Brillouin Scattering Based Fiber Sensors," Sensors **11**, 4152–4187 (2011).
2. B. Lee, "Review of the present status of optical fiber sensors," Opt. Fiber Technol. **9**, 57–79 (2003).
3. K. Hotate, S. Member, and M. Tanaka, "Distributed Fiber Brillouin Strain Sensing With 1-cm Spatial Resolution by Correlation-Based Continuous-Wave Technique," IEEE Photonics Technol. Lett. **14,** 179–181 (2002).
4. S. Uchida, E. Levenberg, and A. Klar, "On-specimen strain measurement with fiber optic distributed sensing," Measurement **60**, 104–113 (2015).
5. T. Horiguchi, K. Shimizu, T. Kurashima, M. Tateda, and Y. Koyamada, "Development of a Distributed Sensing Technique Using Brillouin Scattering," J. Light. Technol. **13**, 1296–1302 (1995).
6. H. Ohno, H. Naruse, M. Kihara, and A. Shimada, "Industrial Applications of the BOTDR Optical Fiber Strain Sensor," Opt. Fiber Technol. **7**, 45–64 (2001).
7. F. Wang, X. Zhang, Y. Lu, R. Dou, and X. Bao, "Spatial resolution analysis for discrete Fourier transform-based Brillouin optical time domain reflectometry," Meas. Sci. Technol. **20**, (2009).
8. Y. Lu, Y. Yao, X. Zhao, F. Wang, and X. Zhang, "Influence of non-perfect extinction ratio of electro-optic modulator on signal-to-noise ratio of BOTDR," Opt. Commun. **297**, 48–54 (2013).
9. J. Geng, S. Staines, M. Blake, and S. Jiang, "Distributed fiber temperature and strain sensor using coherent radio-frequency detection of spontaneous Brillouin scattering," Appl. Opt. **46**, 5928–5932 (2007).
10. Y. Lu, R. Dou, and X. Zhang, "Wideband Dectection of Spontaneous Brillouin Scattering Spectrum in Brillouin Optical Time-Domain Reflectometry," *in proceesings of International Conference on Optical Instruments and Technology*, X. Zhang, ed. (2008), pp. 715818–1-7.
11. Y. Zhang, Z. Ying, G. Tu, X. Zhang, and L. Lv, "Strain variation measurement with short-time Fourier transform-based Brillouin optical time-domain reflectometry sensing system," Electron. Lett. **50**, 1624–1626 (2014).
12. H. Murayama, K. Kageyama, H. Naruse, and A. Shimada, "Distributed Strain Sensing from Damaged Composite Materials Based on Shape Variation of the Brillouin Spectrum," J. Intell. Mater. Syst. Struct. **15**, 17–25, (2004).
13. H. Naruse, M. Tateda, H. Ohno, and A. Shimada, "Dependence of the Brillouin gain spectrum on linear strain distribution for optical time-domain reflectometer-type strain sensors," Appl. Opt. **41**, 7212-7217 (2002).
14. R. Members, "Deformation of the Brillouin Gain Spectrum Caused by Parabolic Strain Distribution and Resulting Measurement System," Ieice trans electron **10**, 2111–2121 (2004).
15. T. Horiguchi, T. Kurashima, M. Tateda, K. Ishihara, and Y. Wakui, "Brillouin characterization of fiber strain in bent slot-type optical-fiber cables," J. Light. Technol. **10**, 1196–1201 (1992).
16. M. T. and T. O. Natsuki NITTA, "Spatial Resolution Enhancement in BOTDR by Spectrum Separation Method," Opt. Rev. **9**, 49–53 (2002).
17. A. W. Brown, M. DeMerchant, and T. W. Bremner, "Spatial resolution enhancement of a Brillouin-distributed sensor using a novel signal processing method," J. Light. Technol. **17**, 1179–1183 (1999).
18. H. Zhang and Z. Wu, "Performance Evaluation of BOTDR-based Distributed Fiber Optic Sensors for Crack Monitoring," Struct. Heal. Monit. **7**, 143–156 (2008).
19. T. R. Parker, M. Farhadiroushan, V. A. Handerek, and A. J. Rogers, "A Fully Ditributed Simultaneous Strain and Temperature Sensor using Spontaneous Brillouin Backscatter," IEEE Photonics Technol. Lett. **9**, 979–981 (1997).
20. M. Nikl and P. A. Robert, "Brillouin Gain Spectrum Characterization in Single-Mode Optical Fibers," J. Light. Technol **15,** 1842–1851 (1997).
21. T. Horiguchi, T. Kurashima, and M. Tateda, "Tensile strain dependence of Brillouin frequency shift in silica optical fibers," IEEE Photonics Technol. *Lett.* **1**, 107–108 (1989).
22. T. Kurashima, T. Horiguchi, and M. Tateda, "Thermal effects on the Brillouin frequency shift in jacketed optical silica fibers," Appl. Opt. **29**, 2219–2222 (1990).

23. Y. Hao, Q. Ye, Z. Pan, H. Cai, R. Qu, and Z. Yang, "Effects of modulated pulse format on spontaneous Brillouin scattering spectrum and BOTDR sensing system," Opt. Laser Technol **46**, 37–41 (2013).
24. F. Hlawatsch, F. Auger, *Time-Frequency Analysis* Concepts and Methods (2008).
25. L. P. Yaroslavsky, "Efficient algorithm for discrete sinc interpolation," Appl. Opt. **36**, 460–463 (1997).
26. K. A. Akant, M. Tech, R. Pande, D. Ph, and S. S. Limaye, "Accurate Monophonic Pitch Tracking Algorithm for QBH and Microtone Research," Pacific J. Sci. Technol. **11**, 342–352 (2010).
27. J. O. Smith, X. Serra, "An Analysis / Synthesis Program for Non-Harmonic Sounds Based on a Sinusoidal Representation," in Processings of International Computor Music Conference, (1987).
28. M. Gasior and J. L. Gonzalez, "Improving FFT Frequency Measurement Resolution by Parabolic and Gaussian Spectrum Interpolation," presented at the 11th Beam Instrumentation Workshop, Knoxville, USA, 3-6May 2004.